Preparation of graphene oxide/epoxy nanocomposites with significantly improved mechanical properties

D. Galpaya, M. Wang, G. George, N. Motta, E. Waclawik, C. Yan*

School of Chemistry, Physics and Mechanical Engineering, Faculty of Science and Engineering, Queensland University of Technology, Brisbane, Australia

The effect of graphene oxide (GO) on the mechanical properties and the curing reaction of Diglycidyl Ether of Bisphenol A/F and Triethylenetetramine epoxy system was investigated. GO was prepared by oxidation of graphite flakes and characterized by spectroscopic and microscopic techniques. Epoxy nanocomposites were fabricated with different GO loading by solution mixing technique. It was found that incorporation of small amount of GO into the epoxy matrix significantly enhanced the mechanical properties of the epoxy. In particular, model I fracture toughness was increased by nearly 50% with the addition of 0.1 wt% GO to epoxy. The toughening mechanism was understood by fractography analysis of the tested samples. The more irregular, coarse and multi-plane fracture surfaces of the epoxy/GO nanocomposites were observed. This implies that the two-dimensional GO sheets effectively disturbed and deflected the crack propagation. At 0.5 wt% GO, elastic modulus was ~35% greater than neat epoxy. Differential scanning calorimetry results showed that GO addition moderately affect the glass transition temperature (T_g) of epoxy. The maximum decrease of T_g by ~7^{o}C was shown for the nanocomposite with 0.5 wt% GO. DSC results further revealed that GO significantly hindered the cure reaction in the epoxy system.

Key words: A. Graphene oxide, B. Epoxy nanocomposite, C. Mechanical performance, D. Cure reaction

---

* *Corresponding author: C. Yan*

Tel +61 7 31386630

Fax: +61 7 31381516

Email address: c2.yan@qut.edu.au

1. INTRODUCTION

Graphene, an atomically thick nanosheet of sp^2-hybridized carbon atoms arranged in a hexagonal two-dimensional (2D) lattice, has generated great interest during the past few years owing to several unique and outstanding properties. Graphene has shown a great potential for various applications such as supercapacitors, lithium ion battery and in high performance polymer composites. Considerable work has already been reported, showing greatly improved electrical, mechanical and thermal properties of neat polymer when reinforced with graphene.[1-4] For instance, Rafiee *et al.*[3] produced epoxy nanocomposites with graphene, single and multi-walled CNTs and compared the mechanical properties at weight fraction of 0.1%. The Young's modulus of their graphene nanocomposite was ~31% greater than the pristine epoxy as compared to ~3 % for single-walled carbon nanotube (CNT). Similarly, model I fracture toughness of epoxy/graphene nanocomposite showed ~53% increase compared to ~ 20% improvement for multi-walled CNT. The superior property improvement of graphene over CNTs was related to the 2D geometry, high specific surface area and better graphene-polymer matrix adhesion due to wrinkled surface texture. However, several key issues need to be resolved in order to attain optimal property enhancement of graphene polymer composite. Similar to any other filler, dispersion and interfacial interactions are the main issues of graphene which directly influence the properties for their composites. Graphene sheets usually tend to form aggregates in solvents and polymer matrices due to strong graphene-graphene intermolecular van der Waals forces consequently this limits dispersion and exfoliation.[5] Poor dispersion and exfoliation of graphene significantly lowers their efficiency as reinforcement. Furthermore, the chemically inert and atomically smooth structure of graphene is highly incompatible with polymer matrix which limits load transfer from polymer matrix to graphene.[6] Hence, homogeneous dispersion of graphene into the matrix, and the strong interfacial interactions between the graphene and the matrix are required in order to efficiently improve the properties of the host matrix.[7]

Compared to graphene, graphene oxide (GO) contains a range of reactive oxygen functional groups such as carboxylic acid, epoxy and hydroxyl group which offer several advantages over graphene. For example, GO is readily dispersible in water, and several organic solvents and polymers.[8] Moreover, functional group attached on the GO surface can make strong interactions with polymer matrix. In addition, bulk quantities of GO can be easily produced by chemically oxidising graphite. Thus, recently several studies have used GO rather than graphene as reinforcing filler for polymer composite.[9-11] However, GO is an insulating material with lower stiffness and strength compared to pristine graphene. Suk *et al.*[12] reported that the Young's modulus of monolayer GO is 207± 23.4 GPa which is only 20% of the value for graphene. Significant toughness and fatigue life improvements through the addition of GO sheets to an epoxy system have been established.[13] The addition of 1wt% GO to an epoxy led to the significant enhancements in flexural strength, flexural modulus and impact strength.[14] Wang *et al.*[15] reported the incorporation of 0.3% of GO into polybenzimidazole (OPBI) enhanced the polymer's Young's modulus by 17%, tensile strength by 33% and toughness by 88%. The extent of oxidation of GO was tailored and its effect on the mechanical performance of polyvinyl alcohol (PVA) has also been investigated. The results showed that the less oxidized GO was more effective than fully oxidized GO in reinforcing PVA.[8] The less oxidized GO could possess higher intrinsic mechanical properties with fewer defects which could be the reason for better enhancement of mechanical performance of PVA nanocomposites.

Epoxy resins are the most important thermosetting materials used in various industrial applications such as in automobile, aerospace, defence *etc*. The study of curing behaviour of epoxy systems is very important because of its close relation between glass transition temperature, mechanical properties and their potential applications. DSC is one of

the most widely used techniques for the analysis of thermal and curing behaviours of thermosetting systems.[16] In the literature, the cure behaviour of epoxy/carbon filler systems has been reported. Qui *et al.*[16] studied the effects of GO on the curing behaviour of tetraglycidyl-4,4'-diaminodiphenylmethane (TGDDM) cured with 4,4'-diaminodiphenylsulfone (DDS) epoxy system. They showed that the oxygen functional groups on the surface of GO acted as catalysts and facilitated the curing reaction and the catalytic effect increased with the GO content. Bortz *et al.*[13] reported similar effect of GO on DGEBA cured with 1,2-diaminocyclohexane (DACH). The acceleration effect has been explained by an increase of oxygen functional groups which could produce a catalytic effect on epoxide ring opening, resulting in higher reaction rates. Teng and co-workers[17] claimed a hindrance effect of graphene on the cure reaction of the DGEBA/DDS epoxy system. In contradiction with Teng's work, Park *et al.*[18] reported a catalytic effect of graphene to speed up the cure reaction rate of di-functional DGEBA/Diethyltoluenediamine (DETDA) epoxy system. Both accelerating[19-21] and retardation[22] effect of CNT on different epoxy systems have been reported by other authors.

However, to date, a relatively limited number of studies have reported on evaluating mechanical performance of GO incorporated epoxy composite and effects of GO on the curing kinetics of epoxy. In the present work, we report the effect of GO on mechanical and thermal behaviour of epoxy nanocomposites with variation of GO weight fraction. Results showed that the modulus, strength and toughness are all simultaneously improved. It was also revealed that GO had a significant influence on the epoxy-amine curing reaction thereby reducing the glass transition temperature of the cured epoxy matrix.

2. EXPERIMENTAL

2.1. Materials

Epoxy resin (Araldite GY 191) used for this study is Diglycidyl Ether of Bisphenol A/F (DGEBA/F) and the curing agent (Hardener HY 956) is a low viscosity aliphatic polyamine (Triethylenetetramine/TETA). Both epoxy resin and curing agent were supplied by CG composites, Australia. Graphite flakes and the other chemicals used such as $KMnO_4$, H_2SO_4, H_3PO_4, HCl, H_2O_2, Acetone, Ethanol and dimethylforamide (DMF) were purchased from Sigma Aldrich (pvt) Ltd, Australia.

2.2. Preparation of graphene oxide

GO was prepared by oxidation of graphite flakes according to the method described by Marcano *et al*.[23] In brief, a mixture of graphite and $KMnO_4$ (Ratio of 1:6) was added into a beaker containing mixture of H_2SO_4:H_3PO_4 (9:1) acids. Then the reaction mixture was stirred while heating at 50^oC for 12 h. The reaction mixture was cooled down to room temperature and poured onto ice with 3 ml of 30% H_2O_2. Then the mixture was sieved through a metal US standard testing sieve (250 μm). The filtrate was centrifuged at 4000 rpm for 30 minutes. The precipitate was washed with DI water, HCl and ethanol. For each wash, the mixture was sieved through US standard testing sieve followed by centrifuging at 4000 rpm for 30 min. The final precipitate was dissolved in DI water and sonicated for 1 h. The sonicated GO dispersion was placed in a deep freezer for 24h followed by freeze drying at -51^oC under vacuum for 72h.

2.3. Preparation of epoxy/graphene oxide nanocomposites

A homogeneous dispersion of GO in acetone (1mg/ml) was obtained by employing an ultrasonicator at high amplitude for 1 h. Then a certain amount of epoxy resin was added and the mixture was stirred for 15 min on a magnetic stirrer. Acetone was evaporated by stirring the mixture at 40^oC for few hours on a hot plate with a magnetic stirrer. The

mixture was placed under vacuum at same temperature overnight for the complete removal of acetone. The stoichiometric amount of hardener was added to the epoxy/ GO mixture at room temperature and mixing was carried out in a high speed shear mixer (Thinky planetary mixer) at 2000 rpm for 5 min. The mixture was then poured into Teflon coated moulds after degassing in a vacuum oven for 30 min. Samples were pre-cured at room temperature for 24h and post-cured at 90^{o}C for 6 h.

2.4. Characterization

2.4.1. Graphene oxide

X-ray diffraction (XRD) powder patterns were taken on a conventional X-ray diffractometer (XRD, PANalytical Cu MPD) using Cu kα radiation. Raman spectra of bulk graphite and GO were recorded from 1250 to 3000 cm^{-1} on a Renishaw inVia Raman Microscope using a 532 nm edge filter laser beam. IR spectra were obtained using FTIR 5700 Nicolet Diamond ATR spectrometer. The spectrum resolution was 4 cm^{-1} in the range from 800 to 4000 cm^{-1}. 64 scans were performed to get the average spectrum. X-ray photoelectron spectroscopy measurements were performed with a Kratos Axis ULTRA X-ray photoelectron spectrometer (XPS) using monochromatic Al-kα radiation (hv = 1486.6 eV). CasaXPS v 2.3.16 software was used to perform curve fitting and to calculate the atomic concentrations. The microstructural characterizations were performed using a JEOL-7001F field-emission scanning electron microscope (FESEM) operated at 15 kV and a JEOL 1400 transmission emission microscope (TEM) operated at 120 kV. Dry GO powder was used for the FESEM analysis. Clear solution of GO in DMF was dropped cast onto carbon coated copper TEM grid for TEM analysis. Samples for atomic force microscope (AFM) imaging were prepared by depositing clear solution of GO (in DMF) on freshly cleaved mica surface. AFM images were taken using a BMT multi-scan AFM with silicon tip. Tapping mode was applied to get the topography of the GO flakes at the scan rate of 1.2 Hz with surface area of 5 x 5μm^2.

2.4.2. Epoxy nanocomposites

Single-edge-notch bending (SENB) specimens were fabricated according to the ASTM D5045-99 standard. A fresh razor blade was utilized to prepare a pre-crack by gently tapping it over a starter notch. Load displacement curves were obtained using Instron tensile machine with the 2 kN load cell at constant cross head speed of 0.5 mm/min. Plane-strain fracture toughness (K_{IC}) was calculated using the load vs. cross head displacement curves as follows;

$$K_Q = \left(\frac{P_Q}{BW^{1/2}} \right) f\left(\frac{a}{W} \right) \tag{1}$$

where P_Q is the maximum load on the load-displacement curve for the SENB specimen; B, W and a are the thickness, the width and the crack length of the specimen, respectively. The term a/W was in between 0.45 to 0.55 for all our samples.

For SENB samples, f is expressed as

$$f(x) = 6x^{1/2} \frac{\left[1.99 - x(1-x)\left(2.15 - 3.93x + 2.7x^2 \right) \right]}{(1+2x)(1-x)^{3/2}} \tag{2}$$

Dog-bone shaped tensile specimens were prepared according to the ASTM D638-10 standard. Tensile strength and elastic modulus were determined from stress-strain curve of composites using the Instron tensile machine with a 2 kN load cell at cross head speed of 0.5 mm/min. Both tensile and bending tests were performed at room temperature and at least five specimens were tested from each sample. The fractured surface images were obtained using FESEM (JEOL-7001F). The fractured ends of the specimens were mounted on aluminium stubs and sputter-coated with a thin layer of

gold to avoid electrostatic charging during examination. TEM and Raman mapping techniques were used to study the dispersion of GO in the epoxy matrix. TEM specimens were prepared by microtoming nanocomposite samples with thickness of 40-70 nm. The ultrathin films were placed on copper grids and examined with JEOL 1400 TEM using an accelerating voltage of 120 kV. For the Raman mapping study, a total of 2500 spectra were collected over a 25 × 25 μm^2 area of the composite surface and at the different depths through the Z axis (0-10 μm) from the surface. The spatial variation of the integrated intensity over the spectral range 1270-1440 cm^{-1} (the location of the carbon related D-peak) and 1500-1700 cm^{-1} (the location of the carbon related G-peak) were used to map the dispersion of the GO in the composite. The typical Raman spectra obtained from the GO regions and epoxy regions, respectively.

Thermal behaviour of the composites was investigated by differential scanning calorimetry (TA Instruments Q100 DSC). Experiments were carried out under nitrogen atmosphere at a scanning rate of 10°C/min from 0 to 280°C. Glass transition temperature (T_g) was obtained from the heat flow curves of fully cured samples. To study the curing behaviour of nanocomposites, samples were prepared as follows. 5-10 mg of freshly prepared sample was added to the hermetic type DSC aluminium pan. Each sample was partially cured by placing in an oven at 90°C and taking out from the oven at different time interval (0, 5, 10, 15, 20, 25, 30 minutes). The heated samples were immediately put in the freezer to stop the reaction. Then, the heat flow curves were obtained for each sample at same experimental conditions used for T_g test as described above. The total heat of reaction (ΔH) was calculated using the heat flow curves and the conversion of reaction (α) was determined at each time, t,

$$\alpha = 1 - \frac{\Delta H_t}{\Delta H_0} \tag{3}$$

3. RESULTS AND DISCUSSION

3.1. Characterization of graphene oxide

Prepared GO is highly hydrophilic and is readily dispersible in water and organic solvents such as DMF, acetone etc. XRD patterns of GO and bulk graphite are shown in Fig. 1(a). A characteristic sharp (002) peak of graphite stacking appeared at 2θ = ~26.5° with a corresponding interlayer spacing of ~0.34 nm. After oxidation of graphite to GO, the peak shifted to a lower angle at 2θ = ~11.0° with a matching spacing of ~0.8 nm which is similar to GO solids reported previously.[24,25] The larger interlayer spacing of GO is due to the large number of polar groups generated between the layers of graphite during oxidation, in which the oxygen and carbon atoms are covalently bonded, leading to an increase in the graphite's crystal lattice length along axis c. The diffraction peak of graphite did not occur in the diffraction spectrogram of GO, indicating that the graphite had been completely oxidized. Raman spectra of graphite and GO are given in Fig. 1(b). The bulk graphite shows two intense bands centred at 1581 cm^{-1} (G band) and 2720 cm^{-1} (2D band). The G band is the response of the in-plane stretching motion of symmetric sp^2 C–C bond. The 2D band is the second order of the D band. A very tiny D band was observed for bulk graphite. This proved the absence of a significant number of defects in the graphite. In contrast, the Raman spectrum of the GO displays an intense D band centred at 1357 cm^{-1} and a G band at 1607 cm^{-1}. The D band arises from the disruption of the symmetrical hexagonal graphitic lattice as a result of internal structural defects, edge defects, and dangling bonds created by the attachment of oxygen-containing functional groups such as hydroxyl and epoxide groups on the carbons.[26] D band intensity is directly proportional to the level of defects in the sample and can also be used as a gauge of degree of functionalization when graphene is chemically modified.[27]

Formation of functional groups during the chemical process was seen by FTIR analysis as shown in Fig. 1(c). There were no peaks observed in the spectrum of pristine graphite, indicating the chemically inert structure of bulk graphite. Chemical and structural changes of graphite upon oxidation are reflected in GO spectrum. A broad band around 3400 cm^{-1} signifies stretching vibration of surface hydroxyls (~ 3400 cm^{-1}) and water absorption (~ 3200 cm^{-1}). The peaks are located at ~1720 cm^{-1} (C=O stretching) from carbonyl and carboxylic groups, at ~ 1200 cm^{-1} (C-OH stretching) from carboxylic groups and at ~1050 cm^{-1} (skeletal C-O or C-C stretching) peak from carbonyl, carboxylic and epoxy groups, which confirms the presence of oxygen-containing functional groups.[28,29] The peak at 1620 cm^{-1} can be assigned to the vibrations of the adsorbed water molecules and also the contributions from the skeletal vibrations of un-oxidized graphitic domains.[30]

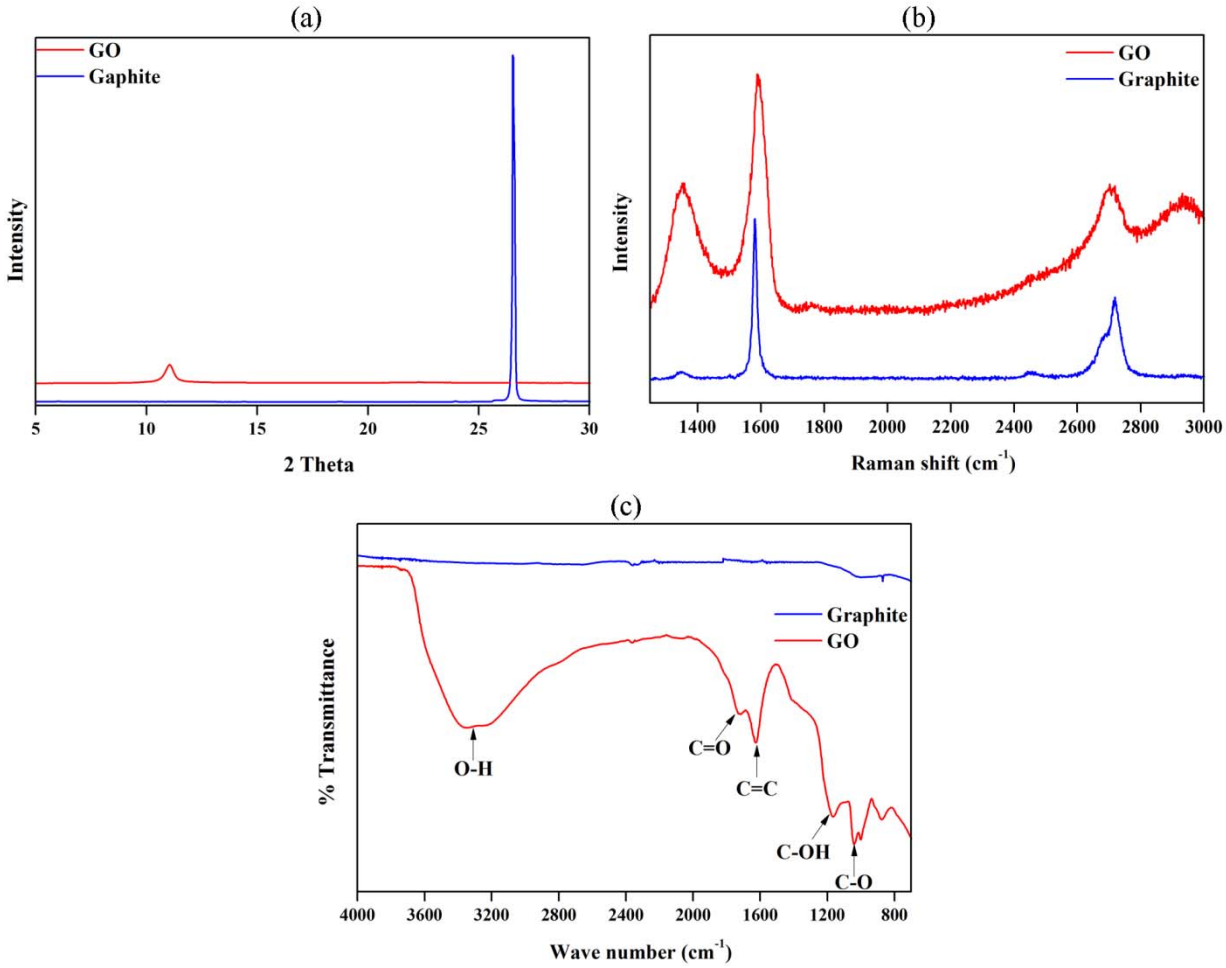

FIG. 1. (a) XRD pattern; (b) Raman spectrum; (c) FTIR spectrum of graphite and graphene oxide.

The C1s XPS spectrum of graphite before chemical treatment is shown in Fig. 2 (a). The peak centred at 284.5 eV corresponds to graphitic carbon (non-oxygenated) and a weak π shake-up band is seen around 291 eV. The atomic composition of graphene oxide was obtained from the XPS survey spectrum and revealed the presence of C (66.6 at %) O (30.4 at %) and small amount of S, N and P (residues from the acids used for the oxidation process). The chemical composition detected for the GO is very similar to reported data in literature.[26,31-33] The detail C 1s and O 1s spectra are shown in Fig. 2 (b) and (c), respectively, of the GO. The C1s XPS data of GO surface clearly displays the presence of four different kinds of carbon atoms. The binding energy of the non-oxygenated carbons (C-C and C-H) bonding are assigned at 284.7 eV. The binding energies at 285.8 eV, 287.5 eV and 288.9 eV can be assigned to carbons attached to carboxylic groups (C*-COOH), carbons in carbon-hydroxyl groups (C*-OH) and epoxy/ether (C*-O) and carboxylate

carbons (O-C*=O), respectively.[25,26] The peaks at 532.4 eV and 533.3 eV in the O1s spectrum of GO (Fig. 2c) can be assigned to contributions from C=O* and C-O*-C/C-O*-H groups, respectively.[26] The peak seen at 534.1 eV may be due to the oxygen from water molecules. All these observations clearly indicate a high degree of oxidation of graphite by the oxidation process.

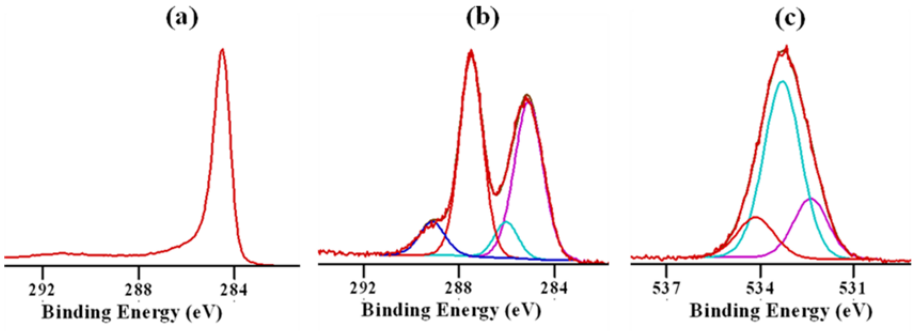

FIG. 2. (a) C 1s XPS spectrum of graphite (b) C 1s and (c) O 1s XPS spectra of graphene oxide.

Fig. 3(a) illustrates the typical SEM image of GO, indicating that GO consists of randomly aggregated, thin crumpled sheets closely associated with each other which are significantly different from graphite flakes. The platelets have lateral dimensions ranging from several hundred nanometers to several micrometers. The morphology and structure of GO was further observed by TEM and the image is shown in Fig. 3(b). As is evident in Fig. 3(b), GO is highly electron transparent. It also clearly shows the wrinkled structure of single or few layers GO which is quite consistent with SEM morphology of Fig. 3(a).

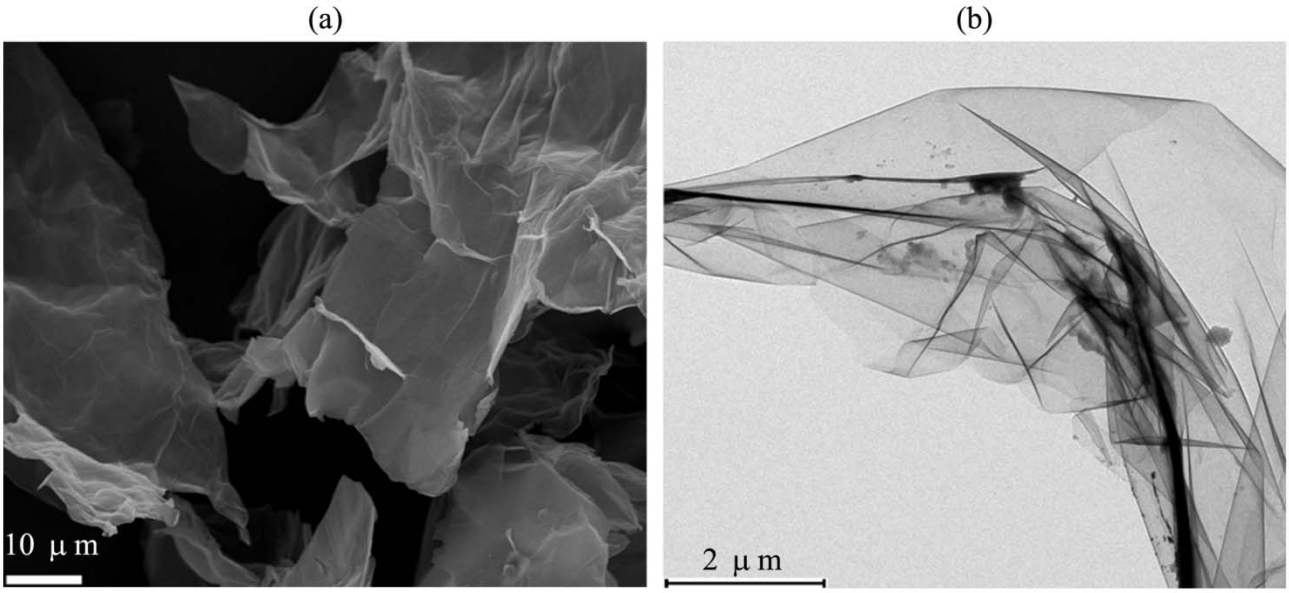

FIG. 3. (a) FESEM (b) TEM images of graphene oxide.

From a tapping mode AFM image of GO on a mica substrate (Fig. 4), the average thickness is ~ 1 nm. This value is very similar to the reported thickness of GO monolayer.[34-36] Compared with the pristine graphene with a thickness of ~ 0.8 nm,[37] the higher thickness of as-made GO is due to the presence of the covalent C–O bonds at both top and bottom surfaces, distorted sp^3 carbon lattices and absorbed contamination.[38-40]

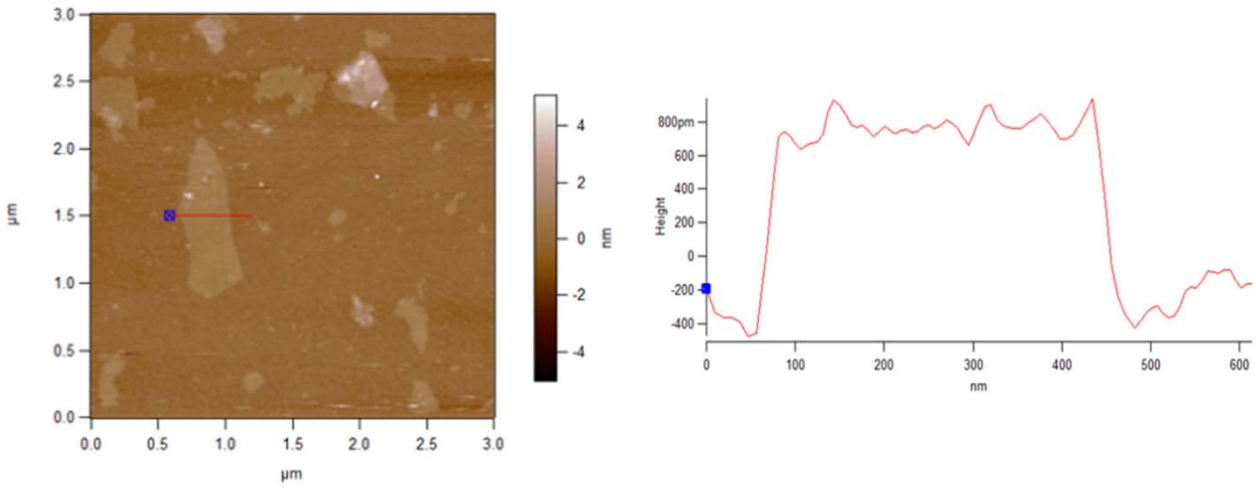

FIG. 4. AFM image of graphene oxide.

3.2. Characterization of graphene oxide/epoxy nanocomposites

3.2.1. Dispersion of GO in epoxy resin

Raman mapping analysis was used to determine the dispersion of GO in epoxy matrix at different concentrations. The typical spectra obtained from the GO region and epoxy region are shown in Fig. 5. The integrated intensity variation of carbon related-D peak (1270-1430 cm^{-1}) and G peak (1500-1650 cm^{-1}) (Fig. 5b) were used to map the dispersion of GO in the nanocomposites, however, for the results presented here only the intregated intensity of the D peak was used. Fig. 6 shows the intensity maps of the D peak over an area of 25 by 25 µm for naocomposites with (a) 0.1wt% (b) 0.3wt% (c) 0.5 wt% (d) 0.7 wt% GO at the depth of 4 µm from the surface. We show here results which are similar what we have found in several random regions of the sample. At low concentrations of GO, distribution of D peak intensity is uniform and in some areas D band is absent due to the lack of GO sheets. This implies that GO sheets are equally dispersed in epoxy matrix. As the GO loading increases, larger several micrometer sized GO agglomerates are visible illustrating poor dispersion of GO at higher loading (Fig. 6c-d).

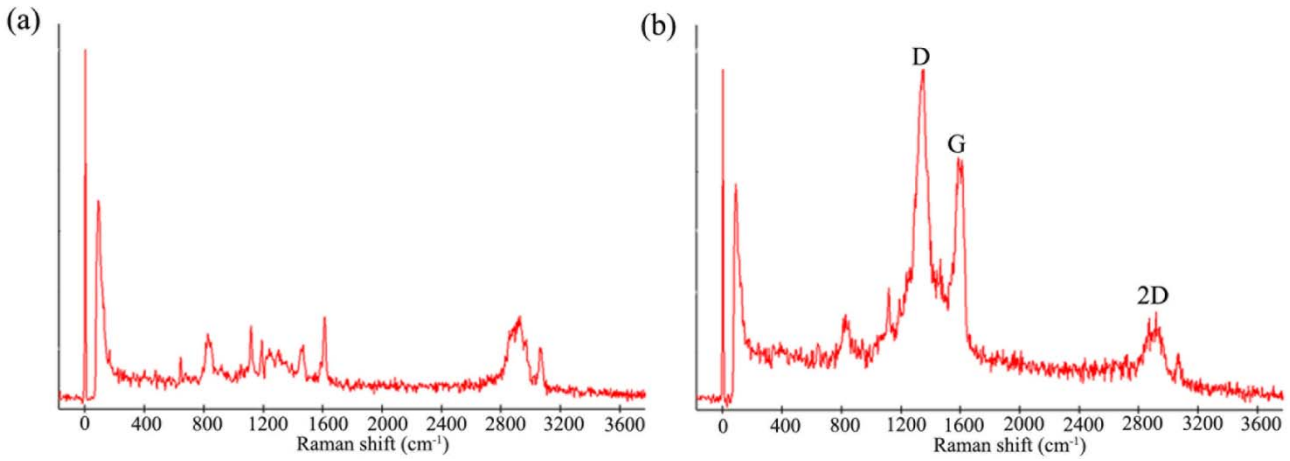

FIG. 5. (a) Raman spectra obtained from epoxy-rich region (b) Raman spectra obtained from GO-rich region showing D, G and 2D bands.

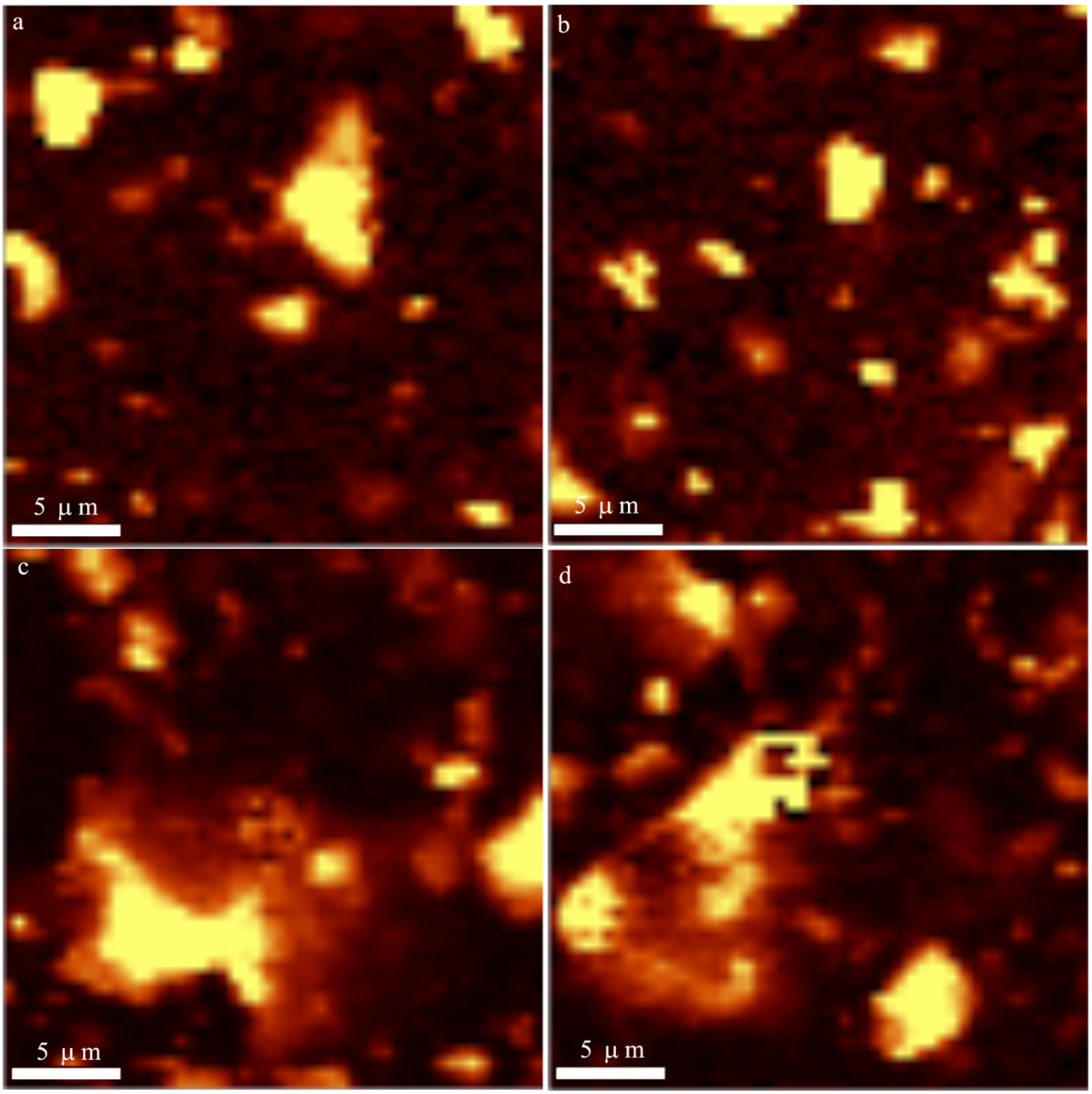

FIG. 6. Distribution of GO in the epoxy matrix obtained by Raman spectroscopy for specimens at depth of 4 μm from the surface with GO loading (wt%) of (a) 0.1, (b) 0.3, (c) 0.5 and (d) 0.7.

Dispersion of GO in epoxy matrix was further studied by TEM analysis and Fig. 7 which shows the TEM image for a specimen with 0.5 wt% GO. As seen in Fig. 7a, GO sheets exhibit considerably exfoliated and dispersed throughout the epoxy matrix although some small aggregations still exist. The number of GO layers could be observed by HRTEM of nanocomposite which was around 7-12 layers as can be seen in the Fig. 7b.

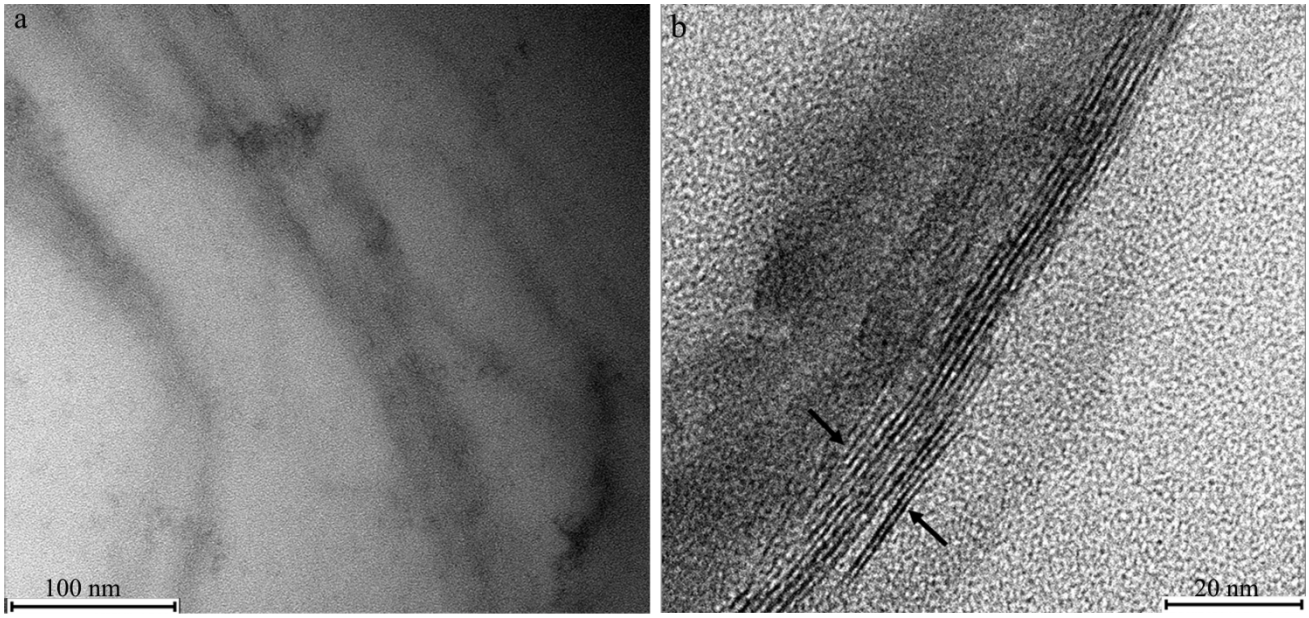

FIG. 7. TEM images of graphene oxide-epoxy nanocomposites at 0.5% GO loading (a) at low (b) high magnification.

3.2.2. Mechanical properties

The mode I fracture toughness (K_{IC}) of neat epoxy and the GO nanocomposites at various loading fractions was determined using the load-displacement curves and results are given in Fig. 8. As it can be seen in the figure, K_{IC} of neat epoxy is ~ 1.34 MPa·m$^{1/2}$, which is comparable to published literature.[1,4] The addition of 0.1 wt% GO into the epoxy matrix enhanced the K_{IC} value of the nanocomposite to ~2 MPa·m$^{1/2}$, which corresponds to a ~50% increase in fracture toughness. It was found that for higher loading fraction, the enhanced ability of GO in K_{IC} became weaker and come near the K_{IC} value of neat epoxy with GO weight fraction of 0.5%. This decrease of the fracture enhancement could be a result of a saturation of the toughening effect and the degradation in the dispersion quality of GO at higher loading fractions as observed in Raman mapping and TEM studies (Fig. 6-7).[13,41] Several researchers have observed the similar behaviour for the composites with higher filler loading fractions.[1,4,13]

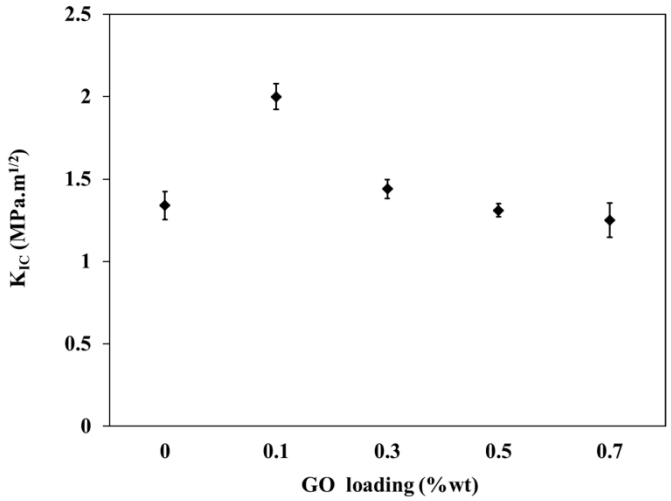

FIG. 8. Plane-strain fracture toughness of graphene oxide-epoxy nanocomposites.

The fracture surfaces were observed using SEM to examine the fractured surface morphology and micrographs are presented in Fig. 9. As shown in Fig. 9a, the fracture surface of neat epoxy is featureless with a smooth surface,

consistent with its typical brittle fracture behaviour. The characteristic brittleness and low fracture toughness of cured epoxy are the result of high crosslink density of cured epoxy which causes low absorption of energy during fracture. With addition of GO, the fracture surface shows the more irregular, coarse and multi-plane surface features as seen in Fig. 9b-d, consistent with higher fracture toughness of nanocomposites compared to neat polymer matrix. Generally, the higher the surface roughness, more fracture energy is dissipated.[5,13] This implies that the two-dimensional GO sheets could slow down the crack propagation by deflection of the propagating crack front. This crack deflection process creates new fracture surfaces, thus increasing the required energy for the crack propagation.[3,4,13,42] However, it was observed that some micro-cracks on the fracture surface with addition of significantly higher amount of GO (see the black arrows in the Fig. 9d). This could indicate more flaws during the crack propagation in the nanocomposite which may result in early fracture of the nanocomposite. This should be the reason for decreasing of K_{IC} of nanocomposites at higher GO loading. According to Wang *et al.*,[41] the enhancement of the epoxy toughness is strongly dependent on the size of the graphene sheet. The smaller the sheet size, better the reinforcement effect. The debonding/delaminating has been reported as one of the key elements of the toughening effect in epoxy matrix. The debonding/delaminating are able to trigger and promote the local plastic deformation of matrix to dissipate fracture energy and subsequently improved fracture toughness.[5]

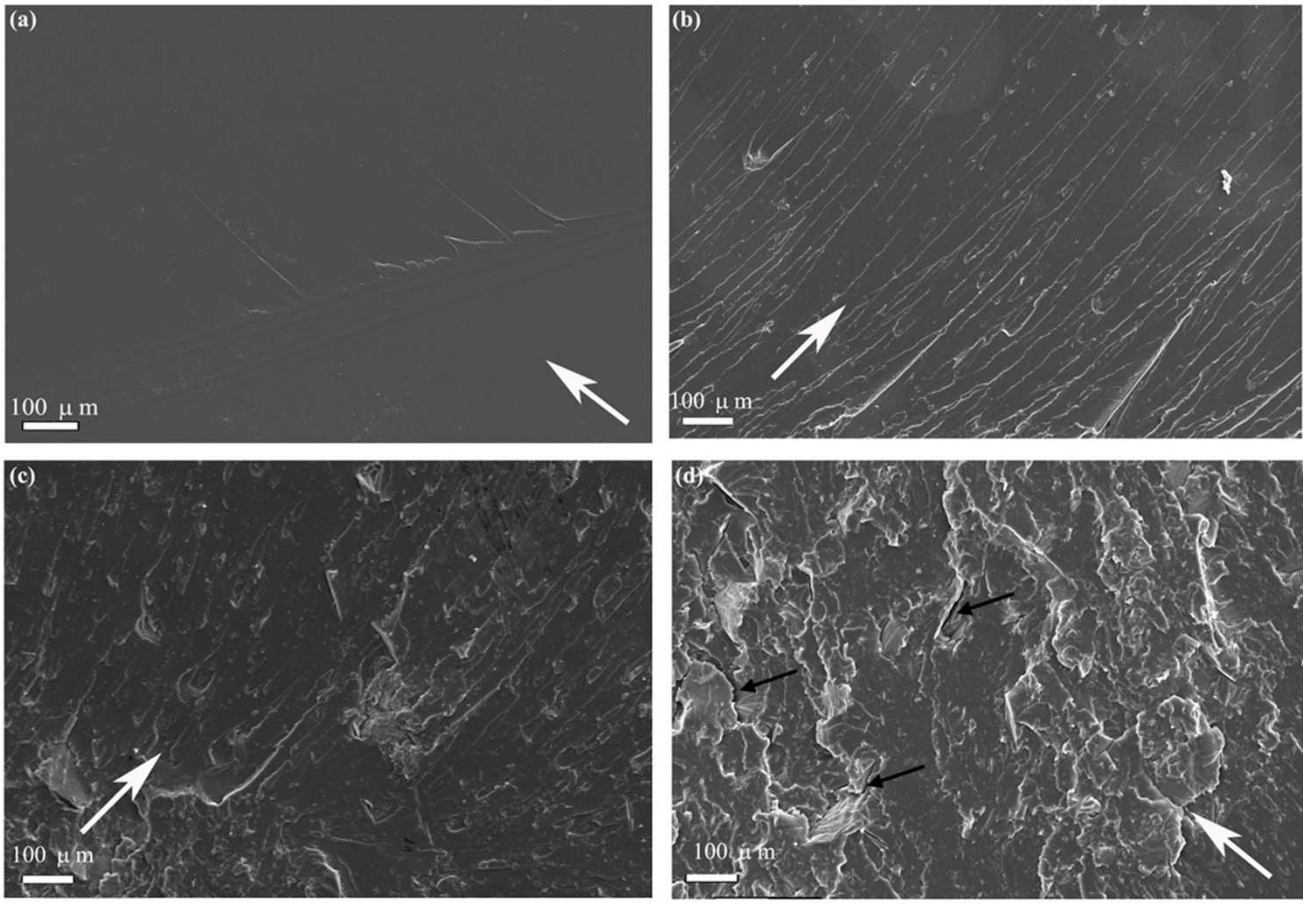

FIG. 9. SEM images of fracture surfaces of SENB specimens: (a) neat epoxy, (b) 0.1 wt%, (c) 0.5 wt% and (d) 0.7wt% GO-epoxy nanocomposites. The white arrows at the bottom of the corners indicate the crack growth direction.

Fig. 10(a) shows variation of ultimate tensile strength and elastic modulus (average value of at least 5 specimens) of neat epoxy and the nanocomposites with different GO content and Fig. 10(b) presents the typical tensile stress-strain curves for neat epoxy and the GO/epoxy composite. From the Fig. 10(a), it can be seen that elastic modulus and ultimate tensile strength of epoxy matrix increased with GO loading. Elastic modulus and tensile strength of neat epoxy are 1.28 GPa and 49.2 MPa, respectively, which are comparable to the values found in literature.[2] Elastic modulus

was enhanced by ~28% at 0.1 wt % GO. Higher loadings also displayed increased tensile stiffness when compared to the neat epoxy but more modest than the weight fraction of 0.1% GO and showed the maximum improvement of 36 % in composite with 0.5 wt% GO compared to the baseline epoxy. Ultimate tensile strength showed a maximum enhancement of about 7% in 0.5 wt% GO nanocomposite compared to control sample. Fig. 10(b) shows that as more GO was incorporated, considerably reduced strains at ultimate strength are observed. The decreased tensile strain of nanocomposites with increasing GO content are typical behaviour of a composite with enhanced strength and stiffness.[43] It is obvious from the results that GO can significantly improve the strength properties of epoxy. Improvement has been credited to (i) high elastic modulus and strength of GO, (ii) better interactions between graphene oxide and polymer matrix and; (iii) uniform dispersion of GO in the epoxy matrix due to abundant functional groups on the GO surface. Similar reinforcing improvement by GO-epoxy nanocomposites has been previously reported.[11,13,14,44] GO contains oxygen containing functional groups across the surfaces which can form covalent bonds with epoxy matrix. Further, distortion caused by oxygen functionalization and extremely small thickness of GO sheets may lead to a wrinkled and rough surface of GO. Together with the wrinkled surface structure of GO which can enhance the mechanical interlocking with the polymer, the surface chemical reactions leads to stronger interfacial interactions and adhesion, and consequently results in efficient load transfer between the GO and the epoxy matrix.[4,9]

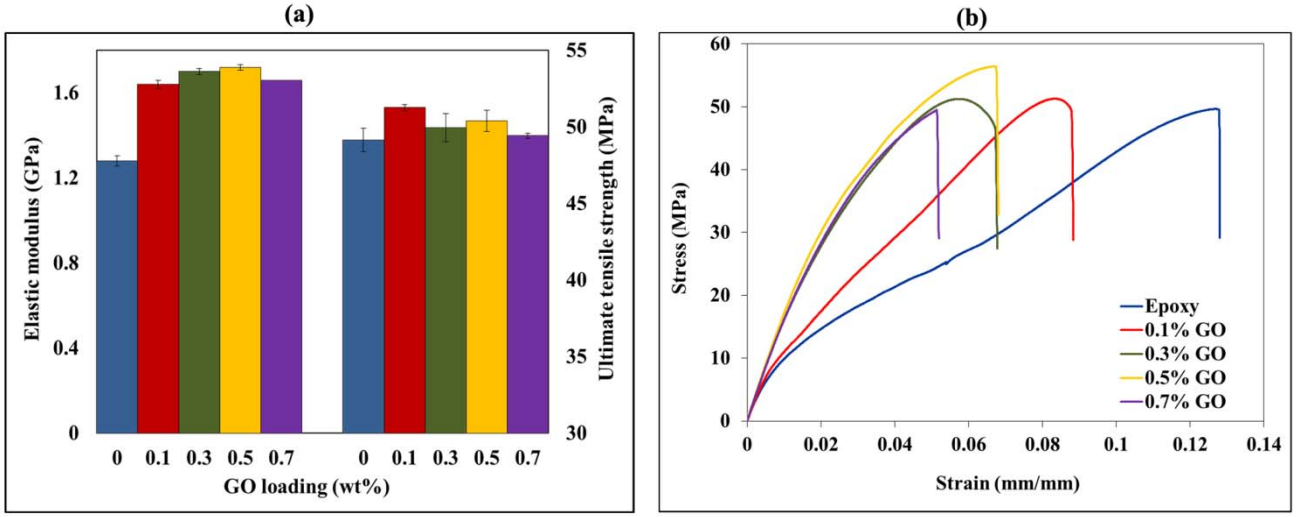

FIG. 10. (a) Elastic modulus and tensile strength, and (b) tensile stress vs tensile strain curves of graphene oxide-epoxy nanocomposites.

3.2.3. Glass transition temperature (T_g) and curing behaviour

Glass transition temperature (T_g) of epoxy and its nanocomposites are shown in Table 1. T_g of pure epoxy is approximately 75.6°C. The T_g of neat epoxy was found to decrease slightly when GO was added to the resin and there was ~4°C decrease in the T_g with the addition of 0.7 wt% GO. Generally, the T_g of composites depends on the balance of two effects, influence on reaction conversion and molecular confinement. Graphene oxide is stiffer than epoxy matrix which could lead to significant confinement on the polymer chains.[45] On the other hand, GO may impede the epoxy curing reaction. This hindrance could be either because of chemical reaction of oxygen-containing functional groups of GO with curing agent (TETA) and/or epoxy resin or covering of reactive sites in the resin and the curative by graphene oxide sheets due to its high surface area. As a result, the optimized ratio of epoxy and curing agent in curing reaction was impacted. This would be expected to reduce the polymer cross-link density and so increase polymer chain mobility. Based on our result, it can suggest that the dominant effect of GO is obstruction of the epoxy curing reaction rather than molecular confinement, leading to positive effect on molecular chain mobility. The less restriction on molecular chain mobility grounds to decrease the T_g.[14,46]

TABLE I. Glass transition temperature T_g of neat epoxy and nanocomposites.

Wt% of GO in epoxy	Glass transition temperature, T_g (^{o}C)
0	75.6
0.1	73.0
0.3	71.5
0.5	68.7
0.7	71.5

The dynamic DSC heat flow curves of the neat epoxy and GO/epoxy systems are illustrated in Fig. 11 (a). The heat of cure (ΔH) in the GO/epoxy nanocomposite is significantly smaller than that of neat epoxy. The ΔH value decreased from 137.1 J/g of neat epoxy to 117.3 J/g of graphene oxide/epoxy nanocomposite with addition of only 0.3% GO. This immediately suggests that GO retarded the cure reaction of epoxy. However, the peak heat flow (T_p), i.e., the temperature of maximum heat flow during the cure reaction, remained unaffected. We have calculated the extent of conversion of the cure reaction (α) as a function of initial curing time using the heat flow curves and Fig. 11 (b) shows the calculated data for neat epoxy and epoxy nanocomposite at 0.3 wt% GO. It can be observed that α of GO /epoxy systems in all time intervals are lower than those of neat epoxy. This suggests that curing reaction of baseline epoxy was slowed down with incorporation of GO into the epoxy matrix. These results further confirmed that GO acts as an obstacle in the curing reaction of epoxy. Retardant effect of GO could arise due to the reaction of oxygen functional groups of GO with amine groups in curing agent resulting in slowing of epoxy curing. The effects of graphene or its derivatives on curing of different epoxy systems have previously been reported. Qui *et al.*[16] reported that GO has an accelerating effects on the curing process of TGDDM/DDS epoxy system. They observed that the oxygen functional groups on the surface of GO acted as catalysts and facilitated the curing reaction and the catalytic effect increased with the GO content. Bortz *et al.*[13] reported similar effect of GO on DGEBA cured with 1, 2- diaminocyclohexane. They observed that the total heat of reaction increased with addition of GO. This effect though appeared saturated at 0.25 wt% GO. Nevertheless, the T_p remained unchanged. The acceleration effect has been explained by an increase of oxygen functional groups which could produce a catalytic effect on epoxide ring opening, resulting in higher reaction rates. Teng *et al.*[17] have observed steric hindrance effect of graphene on epoxy curing reaction. However, Park and Kim[18] reported that graphene acted as a catalyst to speed up the epoxy curing rate.

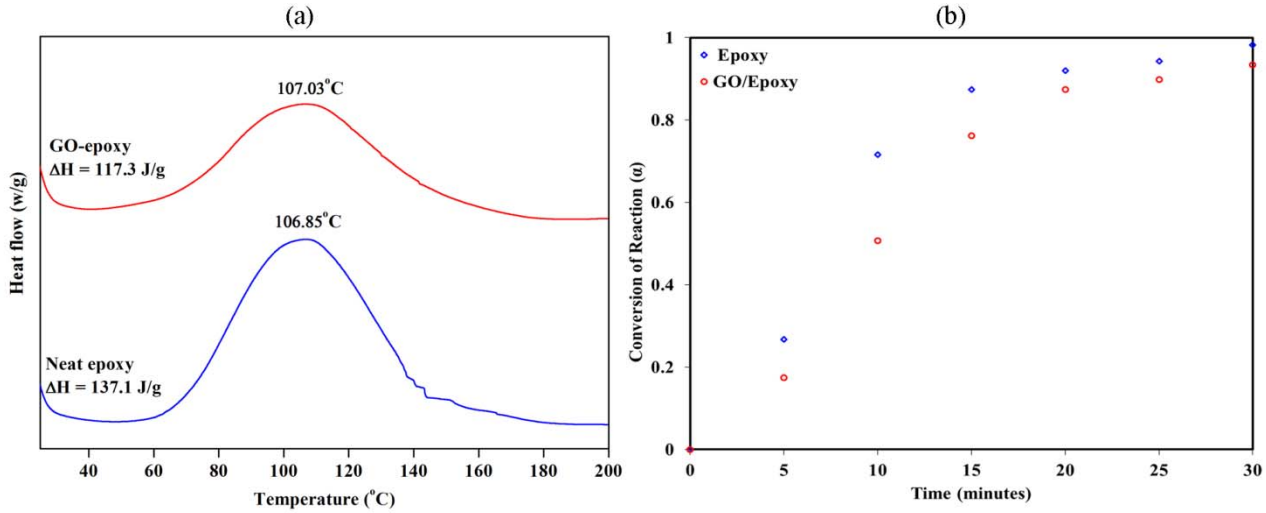

FIG. 11. (a) DSC curves of neat epoxy and graphene oxide/epoxy nanocomposite at partially cure time of 0 (b) Conversion of reaction (α) as a function of partially curing time for neat epoxy and epoxy nanocomposite at graphene oxide loading of 0.3 wt%.

4. CONCLUSIONS

Bulk quantity of GO was prepared by chemical oxidation using modified hummers method. Results showed that graphite could be completely oxidized to GO which is readily soluble in water and organic solvents. The incorporation of very low amount of GO into epoxy matrix has significantly enhanced mechanical performance of epoxy. The mode I fracture toughness increased up to 50% over neat epoxy with 0.1 wt% GO. Elastic modulus showed a steady increase with addition of GO from 0.1 to 0.5 wt% whereas there was no significant effect of GO incorporation on tensile strength. Improvement can be attributed to the superior properties of GO which include their high specific surface area, enhanced interaction/adhesion arising from their oxygen functional groups and wrinkled and rough surface and two-dimensional planar geometry. However, glass transition temperature decreased slightly with increasing GO content in the nanocomposites. Further, the total heat of cure of neat epoxy system is significantly larger than epoxy/GO nanocomposite. This result revealed that GO might retard the cure reaction of epoxy matrix. Retardant effect can cause to reduce the formation of crosslink in the matrix resulting in lower T_g of nanocomposite.

ACKNOWLEDGEMENT

Authors gratefully acknowledge Dr. Barry Wood, University of Queensland, Australia for his invaluable help for XPS analysis. We are thankful to Dr. Llew Rintoul for his help of doing Raman mapping and the Central Analytical Research Facility at Queensland university of Technology for the other characterizations. We thank Queensland university of Technology for financial support.

REFERENCES

[1]A. Zandiatashbar, R. Picu, and N. Koratkar, J. Eng. Mater. Technol. **134,** 031011 (2012).
[2]A. S. Wajid, H. S. T. Ahmed, S. Das, F. Irin, A. F. Jankowski, and M. J. Green, Macromol. Mater. Eng. **298,** 339 (2013).
[3]M. A. Rafiee, J. Rafiee, Z. Wang, H. Song, Z.-Z. Yu, and N. Koratkar, ACS Nano **3,** 3884 (2009).
[4]M. A. Rafiee, J. Rafiee, I. Srivastava, Z. Wang, H. Song, Z.-Z. Yu, and N. Koratkar, Small **6,** 179 (2010).
[5]L.-C. Tang, Y.-J. Wan, D. Yan, Y.-B. Pei, L. Zhao, Y.-B. Li, L.-B. Wu, J.-X. Jiang, and G.-Q. Lai, Carbon **60,** 16 (2013).
[6]Y.-J. Wan, L.-C. Tang, D. Yan, L. Zhao, Y.-B. Li, L.-B. Wu, J.-X. Jiang, and G.-Q. Lai, Compos. Sci. Technol. **82,** 60 (2013).
[7]M. Wang and C. Yan, Science of Advanced Materials **6,** 1501 (2014).
[8]Y. Wang, Z. Shi, J. Yu, L. Chen, J. Zhu, and Z. Hu, Carbon **50,** 5525 (2012).
[9]H. Yang, C. Shan, F. Li, Q. Zhang, D. Han, and L. Niu, J. Mater. Chem. **19,** 8856 (2009).
[10]X.-J. Shen, X.-Q. Pei, S.-Y. Fu, and K. Friedrich, Polymer **54,** 1234 (2013).
[11]Z. Li, R. J. Young, R. Wang, F. Yang, L. Hao, W. Jiao, and W. Liu, Polymer **54,** 5821 (2013).
[12]J. W. Suk, R. D. Piner, J. An, and R. S. Ruoff, ACS Nano **4,** 6557 (2010).
[13]D. R. Bortz, E. G. Heras, and I. Martin-Gullon, Macromolecules **45,** 238 (2011).
[14]Q. Liu, X. Zhou, X. Fan, C. Zhu, X. Yao, and Z. Liu, Polym.-Plast. Technol. Eng. **51,** 251 (2012).
[15]Y. Wang, Z. Shi, J. Fang, H. Xu, and J. Yin, Carbon **49,** 1199 (2011).
[16]S. L. Qui, C. S. Wang, C. G. Liu, X. Y. Chen, H. F. Xie, Y. A. Huang, and R. S. Cheng, eXPRESS Polym Lett **5,** 809 (2011).
[17]C.-C. Teng, C.-C. M. Ma, C.-H. Lu, S.-Y. Yang, S.-H. Lee, M.-C. Hsiao, M.-Y. Yen, K.-C. Chiou, and T.-M. Lee, Carbon **49,** 5107 (2011).
[18]J. K. Park and D. S. Kim, Polym. Eng. Sci. **54,** 969 (2014).
[19]L. Valentini, I. Armentano, D. Puglia, and J. M. Kenny, Carbon **42,** 323 (2004).
[20]H. Xie, B. Liu, Z. Yuan, J. Shen, and R. Cheng, J. Polym. Sci., Part B: Polym. Phys. **42,** 3701 (2004).
[21]J. Wu and D. D. L. Chung, Carbon **42,** 3039 (2004).
[22]J. Bae, J. Jang, and S.-H. Yoon, Macromol. Chem. Phys. **203,** 2196 (2002).
[23]D. C. Marcano, D. V. Kosynkin, J. M. Berlin, A. Sinitskii, Z. Sun, A. Slesarev, L. B. Alemany, W. Lu, and J. M. Tour, ACS Nano **4,** 4806 (2010).
[24]F. Liu, S. Song, D. Xue, and H. Zhang, Adv. Mater. **24,** 1089 (2012).
[25]O. C. Compton, B. Jain, D. A. Dikin, A. Abouimrane, K. Amine, and S. T. Nguyen, ACS Nano **5,** 4380 (2011).
[26]D. Yang, A. Velamakanni, G. Bozoklu, S. Park, M. Stoller, R. D. Piner, S. Stankovich, I. Jung, D. A. Field, C. A. Ventrice Jr, and R. S. Ruoff, Carbon **47,** 145 (2009).
[27]M. Wall, Advanced Material and Process **170,** 35 (2012).
[28]Y. Guo, X. Sun, Y. Liu, W. Wang, H. Qiu, and J. Gao, Carbon **50,** 2513 (2012).
[29]J. Shen, T. Li, Y. Long, M. Shi, N. Li, and M. Ye, Carbon **50,** 2134 (2012).
[30]Y. Si and E. T. Samulski, Nano Lett. **8,** 1679 (2008).
[31]H. A. Becerril, J. Mao, Z. Liu, R. M. Stoltenberg, Z. Bao, and Y. Chen, ACS Nano **2,** 463 (2008).
[32]X. Fan, W. Peng, Y. Li, X. Li, S. Wang, G. Zhang, and F. Zhang, Adv. Mater. **20,** 4490 (2008).
[33]A. V. Murugan, T. Muraliganth, and A. Manthiram, Chem. Mater. **21,** 5004 (2009).
[34]A. J. Glover, D. H. Adamson, and H. C. Schniepp, J. Phys. Chem. C **116,** 20080 (2012).
[35]L. Imperiali, K.-H. Liao, C. Clasen, J. Fransaer, C. W. Macosko, and J. Vermant, Langmuir **28,** 7990 (2012).
[36]Z. Sun, J. Masa, Z. Liu, W. Schuhmann, and M. Muhler, Chem. Eur. J. **18,** 6972 (2012).
[37]K. S. Novoselov, A. K. Geim, S. V. Morozov, D. Jiang, Y. Zhang, S. V. Dubonos, I. V. Grigorieva, and A. A. Firsov, Science **306,** 666 (2004).
[38]S. Stankovich, D. A. Dikin, R. D. Piner, K. A. Kohlhaas, A. Kleinhammes, Y. Jia, Y. Wu, S. T. Nguyen, and R. S. Ruoff, Carbon **45,** 1558 (2007).
[39]K. A. Mkhoyan, A. W. Contryman, J. Silcox, D. A. Stewart, G. Eda, C. Mattevi, S. Miller, and M. Chhowalla, Nano Lett. **9,** 1058 (2009).
[40]M. Cheng, R. Yang, L. Zhang, Z. Shi, W. Yang, D. Wang, G. Xie, D. Shi, and G. Zhang, Carbon **50,** 2581 (2012).
[41]X. Wang, J. Jin, and M. Song, Carbon **65,** 324 (2013).
[42]M. Fang, Z. Zhang, J. Li, H. Zhang, H. Lu, and Y. Yang, J. Mater. Chem. **20,** 9635 (2010).
[43]J. K. Lee, S. Song, and B. Kim, Polym. Compos. **33,** 1263 (2012).

[44]Z. Li, R. Wang, R. J. Young, L. Deng, F. Yang, L. Hao, W. Jiao, and W. Liu, Polymer **54,** 6437 (2013).
[45]S. Wang, M. Tambraparni, J. Qiu, J. Tipton, and D. Dean, Macromolecules **42,** 5251 (2009).
[46]Q. Jingjing, Z. Chuck, W. Ben, and L. Richard, Nanotechnology **18,** 275708 (2007).